3 Wall heat flux calculations from temperature measurements

3.1 Introduction

The following section describes the procedure of the determination of the wall heat flux from the wall temperature measurements using the thin film sensors. First, the heat conduction phenomenon inside the substrate of the gauge, whose application is used in the wall heat flux calculations, is described. Specific analytical solutions underline the importance of the accurate knowledge of the thermal properties of the gauge substrate for accurate wall heat flux calculations. Also, the advantages of the numerical solution of the heat conduction equation based on the Crank-Nicholson scheme that employs no assumptions contrary to the analytical solutions are pointed out. Moreover, the experimental procedure for the determination of the thermal properties of the gauge substrate is presented.

3.2 One dimensional heat conduction

The thin film thickness, which is of the order of *0.2μm* for the VKI gauges, is small enough to not affect the temperature history of the substrate surface; the heat conduction during the test is taken into account only inside the substrate thickness, whose value usually ranges from a few millimeters to a few centimeters, depending on the substrate material. Additionally, the thermal conductivity of the film (Table 18-1) is much higher than the one of the substrate and the frequency response of the film is a lot higher than the frequency of the possible periodic phenomena identified in the experimental environment under investigation. Thus, the high response of the thin film and its small thickness (compared to the substrate) reinforce the assumption that the thin film thickness has a negligible effect on the heat conduction process (Schultz and Jones, 1973).

The one dimensional heat conduction equation for a multi-layer substrate system is expressed in Eq. (3):

$$\frac{\partial T(x,t)}{\partial t} = \alpha(x)\frac{\partial^2 T(x,t)}{\partial x^2} \quad . \tag{3}$$

The thermal properties, such as the thermal diffusivity, $\alpha(x)$, depend only on the considered location x inside the substrates for small temperature changes such as the ones used for the following applications (of the order of *100K*), while the temperature T is a function of the location x and the time t. A two-layer substrate gauge is shown in Figure 1-2.

The necessary boundary conditions to solve Eq. (3) in order to calculate the wall heat flux from the wall temperature measurements with the thin film gauges are:
i) at a given substrate depth x (distance from the wall), the temperature can be considered as constant during the short testing time (semi-infinite substrate hypothesis – paragraph 3.7.1.2), by selecting the total thickness of the substrates enough big (paragraph 2.2.4),
ii) the wall temperature increase during the experiment,
iii) at the substrate interface $x=L$, the values of heat flux and temperature for the two bordering substrates are equal:

$$-k_1\left(\frac{\partial T_1(t)}{\partial x}\right)_{x=L-} = -k_2\left(\frac{\partial T_2(t)}{\partial x}\right)_{x=L+} \quad , \tag{4}$$

$$T_1(x=L-,t) = T_2(x=L+,t) \; , \tag{5}$$

where the indexes *1* and *2* stand for the first layer and the second layer of the gauge respectively and $L-$, $L+$ refer to grid area on [L and (L-Δx)], [L and (L+Δx)] respectively,

iv) the initial temperature everywhere in the gauge substrate is uniform and known.

The heat flux at the wall is computed thanks to the Fourier law:

$$Q_W(t) = -k_1\left(\frac{\partial T_1(t)}{\partial x}\right)_{x=0} . \tag{6}$$

3.3 Analytical solutions for single-layer gauges

The single-layer gauges consist of only one substrate material, usually Macor (at VKI) or Pyrex or quartz, which is an insulator from electrical and thermal point of views. As an electrical insulator, the substrate does not interfere with the thin film sensor's electrical signals and thus insulates all gauges from each other. As a thermal insulator, not only the two dimensional conduction is limited and considered negligible for the wall heat flux calculations, but also the semi-infinite condition is easily achieved during a test (paragraph 3.7.1.2).

3.3.1 Solution in the Laplace domain

The solution of Eq. (3) in the Laplace domain, which gives the wall heat flux, is described in Eq. (7), where p is the Laplace variable, $p = e^{\sigma + j\omega}$ (Schultz and Jones, 1973):

$$\overline{T_W}(p) = \frac{\overline{Q_W}(p)}{\sqrt{\rho ck}\sqrt{p}} . \tag{7}$$

If p reduces to $p = e^{j\omega}$, namely if the domain is restricted to the Fourier domain of periodic signals, Eq. (7) reduces to:

$$\hat{Q}_W(p) = \frac{\pi}{4}, \quad Q_W(p) = \sqrt{\rho ck}\sqrt{j\omega} , \tag{8}$$

where $\hat{Q}_W$ and Q_W are respectively the phase and the magnitude of the wall heat flux and $\omega = 2\pi f$ is the pulsation in *rad/s*. The value of the heat flux at the wall depends only on the physical constant $\sqrt{\rho ck}$, i.e. the so-called thermal product. For this reason, the accuracy on the heat flux is directly linked to the accuracy on the thermal product of the substrate. In addition, if one considers a low frequency wall temperature fluctuation, the amplitude of the corresponding heat flux will be lower than that of a high frequency temperature fluctuation of the same magnitude, according to Eq. (8). As an example, it is interesting to compare two temperature fluctuations occurring at a frequency of *6.9kHz* (that corresponds to blade passing frequency in CT3) and 1 Hz of the same amplitude: the ratio of the magnitude of the two corresponding surface heat flux fluctuations is *83*.

3.3.2 Step function in wall heat flux

In the case of a step function in wall heat flux (constant heat flux with time), the wall temperature in the time domain is given by Eq. (9) (Schultz and Jones, 1973):

$$T_W(t) - T_0 = \frac{2Q_W}{\sqrt{\pi}}\frac{\sqrt{t - t_0}}{\sqrt{\rho ck}} . \tag{9}$$

This can be very convenient to determine the thermal product $\sqrt{\rho ck}$ when a known heat flux is applied or vice-versa. This concept is mainly used for the calibration of Macor gauges

using electrical heating by joule effect (electrical discharge calibration method, Schultz and Jones, 1973 – paragraph 3.8). Note that the time t_0 corresponds to the beginning of the heat flux step. T_0 is the initial temperature of the gauge's substrate.

3.3.3 Step in fluid temperature

In case of a step function in the fluid temperature, which corresponds to a constant heat transfer coefficient h, there is an analytical solution for the wall temperature history $T_W(t)$ (Schultz and Jones, 1973):

$$\frac{T_W(t)-T_0}{T_{GAS}-T_0} = 1 - e^{(\beta^2)} erfc(\beta), \qquad \beta = \frac{h\sqrt{t-t_0}}{\sqrt{\rho c k}} \cdot \tag{10}$$

This solution models in the best way the measurements performed in short duration wind tunnels. It is also used to determine experimentally the thermal product $\sqrt{\rho c k}$ of the substrate, when the gauge is abruptly submitted to a uniform air jet.

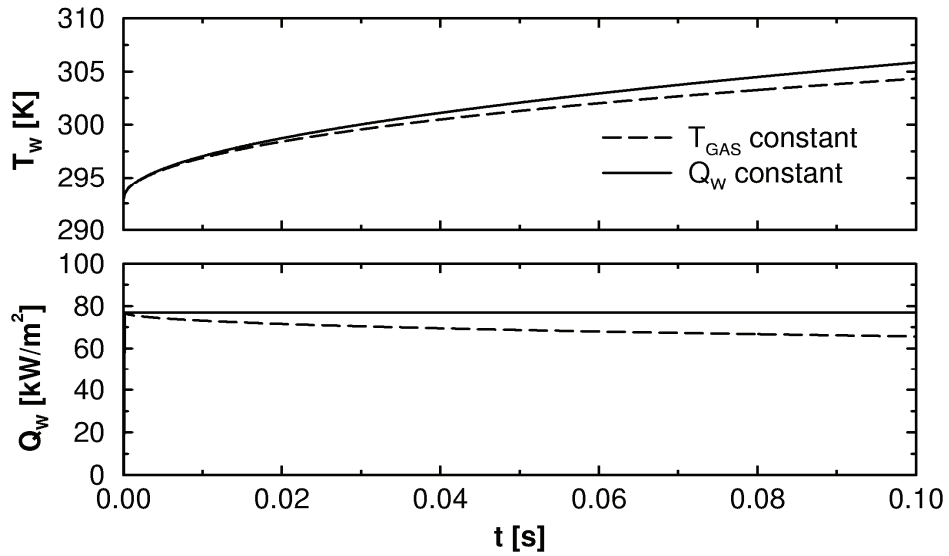

Figure 3-1: Numerically generated wall temperature signals that correspond to constant gas temperature and constant wall heat flux cases

Two numerically generated examples of wall temperature and their corresponding wall heat flux histories are presented in Figure 3-1. The first case (solid line) corresponds to a constant heat flux of $77kW/m^2$ and the second case (dashed line) characterizes the constant gas temperature case. The heat transfer coefficient of the second case is equal to that of the constant heat flux case for time zero, i.e. $1kW/(m^2K)$. The value of the thermal product of the substrate is chosen equal to $2139\ J/(m^2Ks^{0.5})$ that corresponds to a Macor substrate. Note that for short times, such as less than *20ms*, the difference between the two wall heat fluxes for this specific case is around *7%*, which could eventually be considered low enough to assimilate the constant gas temperature case to a constant wall heat flux case in specific applications described later.

3.4 Analytical solutions for two-layer gauges

An analytical solution of Eq. (3) exists for the case of a two-layer gauge submitted to a constant wall heat flux; it is given in Eq. (11), (Doorly & Oldfield, 1986):

$$\Delta T_W = \frac{2Q_W \left\{ \sqrt{\frac{t'}{\pi}} + 2\sum_{n=1}^{\infty} A^n \left[\left(\frac{t'}{\pi}\right)^{\frac{1}{2}} \exp\left(-\frac{n^2 L^2}{\alpha_1 t'}\right) - \frac{nL}{\sqrt{\alpha_1}} erfc\left(\frac{nL}{(\alpha_1 t')^{0.5}}\right) \right] \right\}}{\sqrt{(\rho ck)_1}} , \quad (11)$$

where: $A = \frac{1-\sigma}{1+\sigma}$, $\sigma = \frac{\sqrt{(\rho ck)_2}}{\sqrt{(\rho ck)_1}}$, $\Delta T_W = T_W - T_0$, $t' = t - t_0$. (12)

The value of the wall heat flux depends only on the three physical constants $\sqrt{(\rho ck)_1}$, $\sqrt{(\rho ck)_2}$, which are the thermal products of the first and the second substrate, and *L*, which is the thickness of the first one. For this reason, the accuracy on the heat flux is directly linked to the accuracy of the three above parameters. When the wall temperature rise is plotted in function of $\sqrt{t - t_0}$, the response of the successive substrates can be approximated, according to Eq. (13), by two straight lines (see also Figure 3-2):

$$T_W(t) = \frac{2Q_W}{\sqrt{\pi}\sqrt{(\rho ck)_2}} \sqrt{t - t_0} + Q_W \frac{L}{k_1}\left(1 - \frac{(\rho ck)_1}{(\rho ck)_2}\right) . \quad (13)$$

The first slope is inversely proportional to the thermal product of the first layer. Similarly, the second slope is related to the thermal product of the second layer.

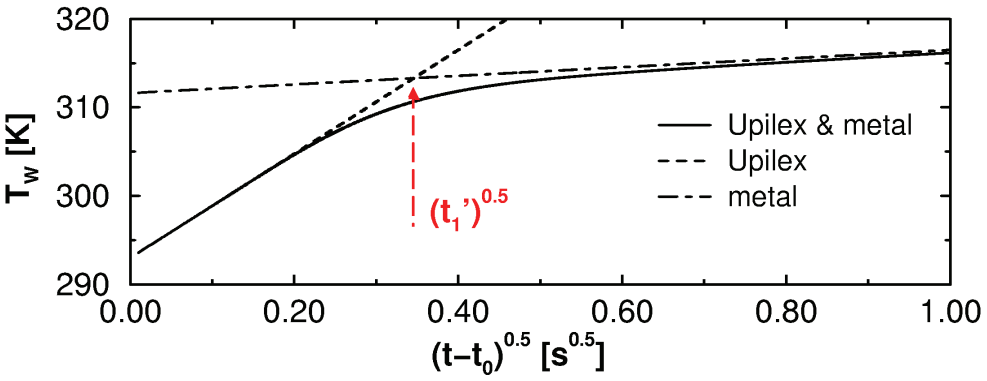

Figure 3-2: Approximation of the wall temperature history by two slopes for the case of constant wall heat flux

The time at which the two lines intersect allows the determination of the first layer thickness. In addition, the intersection between these two slopes, $(t_1')^{0.5}$, the "switch point", characterizes the thickness of the top layer. The so-called thermal thickness parameter, L/k_1 defined in Eq. (14):

$$\frac{L}{k_1} = \frac{2}{\sqrt{\pi}} (t_1')^{0.5} \frac{\left(\sqrt{(\rho ck)_1}\right)^{-1} - \left(\sqrt{(\rho ck)_2}\right)^{-1}}{1 - \sigma^{-2}} . \quad (14)$$

In Figure 3-2, Upilex and conventional steel with nickel 20% (Table 18-1) have been selected as the materials of the first and second layer respectively ($\sqrt{(\rho ck)_{1,2}}$ = *692, 8327 J/(m²Ks^0.5)*). The thickness of Upilex is *150µm*, and the wall heat flux is *36kW/m²*.

3.5 From step in fluid temperature to step in wall heat flux

In the case of two-layer gauges, the only analytical solution available is, to the best authors' knowledge, for a constant heat flux. However, by using a superposition technique as described by Piccini et al. (2000) the constant gas temperature case can be 'corrected' to a constant heat flux case. The technique consists in determining the transfer function that will transform the variable heat flux obtained during the constant gas temperature case (Eq. (15)) into a constant heat flux (Eq. (16)) preferably equal to the heat flux at time $t\text{-}t_0=0$ of the constant gas temperature case:

$$Q_1(t) = Q_{W,TGAS\ =CT}(t) = h(t)\left[T_{GAS} - T_{W,TGAS\ =CT}(t)\right], \tag{15}$$

$$Q_2 = Q_{W,CT} = h_0\left(T_{GAS} - T_0\right) \quad . \tag{16}$$

To apply a transfer function in the discrete time domain, a convolution is performed between the discrete heat flux and the discrete transfer function (a product in the frequency domain becomes a convolution in the time domain). At time $t=m\Delta t$, for $m = 0, N$ one has:

$$\sum_{i=0}^{m} b(i) Q_1(m-i) = Q_2(m) = CT \quad , \tag{17}$$

where $b(m)$ are the coefficients of the transfer function in the time domain. Equation (17) can be written for all successive time steps (Eq. (18)) and solved to obtain the coefficient $b(m)$ (see Piccini et al., 2000). Then the new generated wall temperature history is given in Eq. (19):

$$b(m) = \frac{Q_2 - \sum_{i=0}^{m-1} b(i) Q_1(m-i)}{Q_1(0)} \ , \tag{18}$$

$$T_{W,2}(m) - T_0 = \sum_{i=0}^{m} b(i)\left[T_{W,TGAS\ =CT}(m-i) - T_0\right] . \tag{19}$$

Note that the above analysis is applicable for any kind of thin film gauge, single or two-layer. The relationships are successfully tested for the example of Figure 3-1: a numerically generated wall temperature signal (dashed line in Figure 3-1), which corresponds to a constant heat transfer coefficient, is transformed to a wall temperature signal (superposed signal, solid line). The superposed signal corresponds to a constant wall heat flux. A characteristic of this technique is that it does not depend on the value of the heat transfer coefficient, h (Eq. (18)). However, the magnitude of the constant wall heat flux *does* indeed depend on the corresponding initial value of the time dependent h (for time $t\text{-}t_0=0$). Thus, for the example of Figure 3-1, this initial value of h for the case of constant wall flux corresponds to the constant h case.

The above technique was also successfully tested for the two-layer gauge by Billiard et al. (2002). There is no analytical solution to the author's knowledge that gives a wall temperature signal corresponding to a constant heat transfer for the case of two-layer gauge, therefore, a suitable test is produced: the gauge is submitted to a step of a uniform air jet (constant gas temperature case). The recorded signal and the corresponding calculated wall heat flux (by using the numerical solution based on the Crank-Nicholson scheme) are shown in Figure 3-3 (solid black line). The superposition technique generates a wall temperature signal, which corresponds to a constant wall heat flux, also shown in Figure 3-3 (dashed red line). Once more, the initial value of h for time $t\text{-}t_0=0$ for the superposed signal is equal to the constant h of the test.

At this point, note that an accurate calculation of the wall heat flux requires an accurate knowledge of the two thermal products and the thickness of the first layer. Nevertheless, the superposed temperature signal requires no knowledge of the above three parameters in order to be reconstructed accurately (see Eq. (18) and Eq. (19)). This conclusion is used for the calibration of

the two-layer gauge (described in 3.9.2). However, the wall heat fluxes given in Figure 3-3 are calculated after the calibration of the gauge.

The application of the above superposition technique is always combined with the analytical solution from Eq. (11) during the calibration of the two-layer gauge: together, they can substitute the general numerical solution described in the next paragraph for the specific constant gas temperature case. Note that the constant gas temperature case is experimentally generated by a uniform air jet.

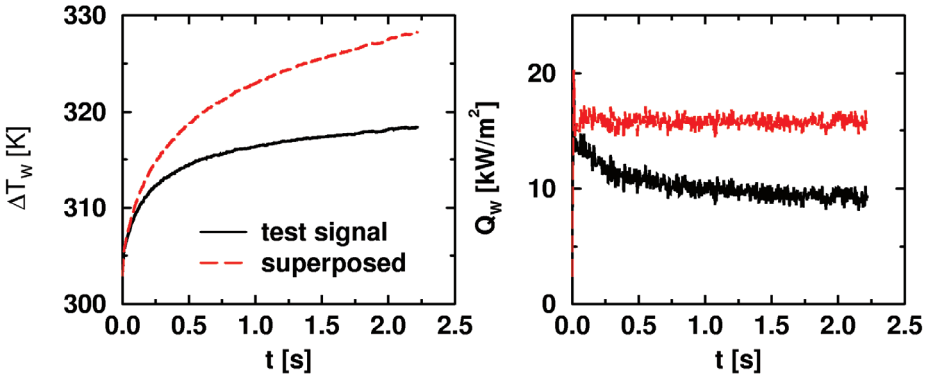

Figure 3-3: Application of the superposition technique on a two-layer gauge

3.6 Numerical solutions

As mentioned before, the wall heat flux is obtained by solving the one dimensional (1D) unsteady conduction equation across the successive substrates (Eq. (3)) with temperature histories or heat flux histories at the wall and at a given depth as boundary conditions. The temperature history inside the substrate is then obtained and the wall heat flux is given by Eq. (6). The initial temperature distribution inside the substrate at time zero is assumed uniform because the substrate is under thermal equilibrium before the test.

The finite difference Crank–Nicholson scheme consists of a weighted arithmetic average of the explicit and implicit formulation of the space derivative (Anderson, 1985) and is applied on Eq. (3):

$$\frac{T_j^{m+1}-T_j^m}{\Delta t}=\eta\left[\frac{\frac{\alpha^k\left(T_{j+1}^{m+1}-T_j^{m+1}\right)}{\Delta x_j}-\frac{\alpha^k\left(T_j^{m+1}-T_{j-1}^{m+1}\right)}{\Delta x_{j-1}}}{\frac{\Delta x_{j-1}}{2}+\frac{\Delta x_j}{2}}\right]+(1-\eta)\left[\frac{\frac{\alpha^k\left(T_{j+1}^{m}-T_j^{m}\right)}{\Delta x_j}-\frac{\alpha^k\left(T_j^{m}-T_{j-1}^{m}\right)}{\Delta x_{j-1}}}{\frac{\Delta x_{j-1}}{2}+\frac{\Delta x_j}{2}}\right], \quad (20)$$

where k takes the value *1* or *2* for the first and the second layer respectively, m for the time step. Note that η is a numerical parameter that controls the stability of the scheme. This stability is ensured unconditionally if η is larger than 0.5, i.e. time step and space step are completely decoupled. If the unknowns at time $m+1$ are expressed as a function of the computed solution at time m, a tri–diagonal system is obtained that can be efficiently solved with existing algorithms. The solution provides the distribution of temperature in the gauge substrate at time step $m+1$. Equation (20) is used for all the mesh points for both layers, except at the interface L of the two layers, where the temperature and the heat flux of the first layer are imposed equal to the second layer [Eq. (4), (5)]. The mesh of the second layer, Δx^2, compared to the first layer, Δx^1, should not be chosen more than few percent different at the interface, so that a high gradient of the substrate conductivity results in low temperature gradient. Note that the thermal properties of the substrate materials are considered constant with time for cases where the substrate temperature change is of the order of few K; variations of the thermal properties of Pyrex, quartz and Macor as a function of substrate temperature are given by Miller (1981).

A data reduction program based on the above numerical solution has been produced and successfully validated versus several test cases for which analytical solutions exist for one and two layers of substrate. The wall heat flux is computed thanks to the Fourier law by using the first and the second grid point on and next to the gauge surface respectively. An example is given in Figure 3-4, where the wall temperature distribution shown in Figure 3-2 is used as a boundary condition of Eq. (3). The corresponding calculated constant wall heat flux ($36\ kW/m^2$) is shown in Figure 3-4. This solution is independent of the number of grid points (*3000* points is a typical value for 10^{-4} to 10^{-5} *sec* of time step). Note, that this data reduction technique can be used to compute the wall heat flux from the corresponding temperature history and vice-versa without any restrictive hypothesis on the boundary conditions. Thus, the wall heat flux can be determined not only for a step in wall heat flux or a step in gas temperature, but also for any kind of applied unsteady flow on the gauge surface.

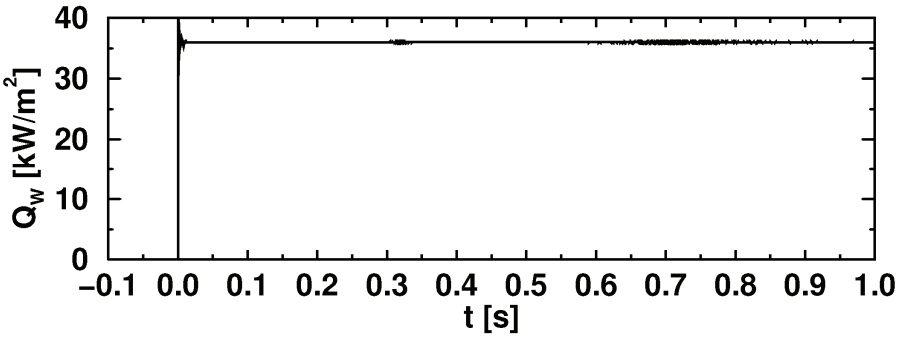

Figure 3-4: Validation of the numerical solution by using as a boundary condition the generated wall temperature history from the analytical solution

3.7 Experimental environment

The importance of the accurate knowledge of the thermal products of the substrates is already mentioned in Eq. (7) for single-layer gauges and Eq. (13) for two-layer ones, as well as of the thickness of the first layer, for accurate wall flux calculations. Thus, the choice of the substrate materials (and the first layer thickness) must be properly made and quantified through a calibration procedure.

3.7.1 Thermal insulator as a substrate

The analytical solutions, presented before, clearly indicate that for a specific value of wall flux, the lower the thermal product of the substrate is, the faster the wall temperature rises. The latter is the quantity measured during the test, thus, the higher the temperature signal, the better the data acquisition will be resolved. In addition, the higher the signal to noise ratio, the smaller is the noise on the wall heat flux calculations. However, the use of an insulating material as a substrate is the best choice not only for the measured signal, but also for several other reasons described below.

3.7.1.1 One dimensional hypothesis

The wall heat flux is determined from Eq. (3), which describes the heat conduction in the substrates assuming one dimensional behavior. No lateral conduction effects are considered. Therefore, the substrate material should be a thermal insulator (low thermal diffusivity) in order to minimize lateral conduction during the test time.

3.7.1.2 Semi-infinite hypothesis

The whole procedure described above for the wall heat flux determination from the wall temperature history is based on the condition that the total depth of the substrates is such that at a

given distance x from the wall, the temperature can be considered as constant (semi-infinite hypothesis). Schultz and Jones (1973) propose a criterion for the minimum value of the substrate thickness that is required to satisfy the semi-infinite condition for a single-layer gauge based on the constant heat flux solution. This thickness L is defined as:

$$\frac{T(x)}{T_W} \le 1\% \leftrightarrow x \ge L : L = 3.16\sqrt{\alpha t} \ ,$$
$$\frac{Q(x)}{Q_W} \le 1\% \leftrightarrow x \ge L : L = 3.74\sqrt{\alpha t} \ , \qquad (21)$$

where T_W and Q_W stand for the temperature and the heat flux at the wall ($x=0$), α stands for the thermal diffusivity of the substrate and t for the time during which the Q_W is applied. Thus, an insulator with smaller α satisfies the semi-infinite condition with smaller required L than a conductor.

3.7.2 Flat plate analysis – Curved surfaces

Equation (3) assumes that the wall on which the gauges are deposited is flat and no surface curvature effects are taken into account for the wall heat flux calculations. All the analytical and numerical solutions that are presented in the previous paragraphs are based on the flat plate analysis. In case that the surface is actually curved, errors on the wall heat flux calculations will be introduced and depend on how far the heat penetrates into the substrate relative to the radius of curvature at the wall (more information can be found in paragraphs 10.3 and 10.5).

In addition, the first layer sheet is easily glued onto blade walls that can be developed into flat surfaces such as vanes. However, when the blade geometry is three dimensional, such as the one of the rotor blades, the instrumented first layer sheet is usually cut into several smaller pieces to facilitate the gluing procedure.

3.7.3 Nominal and calibrated thermal properties

Materials such as quartz, Plexiglas and Macor are often used as substrates for the single-layer gauges due to their low thermal conductivity. The nominal values of their properties are listed in Table 18-1. However, not only the thermal product of the same kind of material could deviate from one batch to another, but mainly its value is influenced during the manufacturing of the gauge. The sensor, which is the thin film of highly conductive material such as platinum or nickel, is painted and then cured in an oven. The changes on the thermal product of the insulating substrate are attributed to the diffusion of the metallic film during its curing process (Miller, 1981). Hence, an experimental determination of the thermal product, the thermal product calibration, is necessary for the next study.

As far as the two-layer gauge is concerned, the first layer that carries the sensor is glued on the second layer by the use of a double-sided adhesive sheet, whose thermal product is expected to have the same value as the first layer. (The latter statement is also experimentally checked in paragraph 3.9.3.) Thus, the gauge has two layers from a thermal point of view, and the first insulator together with the glue is considered as one layer. In addition, the thickness of the first layer (insulator and glue) could eventually be influenced during the manufacturing of the gauge. As a result, the first layer thickness (insulator plus glue) should be experimentally quantified during the calibration procedure of the thermal products of the two layers.

3.7.4 Zero time: experimental step in wall heat flux for calibration

The constant wall heat flux solutions for the heat conduction in single or two-layer gauges can be used for the determination of the thermal products and the first layer thickness,

when the heat flux source is well known. This wall heat flux can be achieved by heating the film sensor by Joule effect or by means of radiation effect, or conduction effect. The result is influenced by the value of t_0, the time at which the wall temperature starts to rise. Experimentally, it is difficult to generate a step wall heat flux function for long time (more than few milliseconds) and the time t_0 cannot always be determined with accuracy. However, the single-layer gauge is successfully calibrated by the use of the Joule effect (Denos, 1996 – paragraph 3.8).

3.7.5 Uniform thickness of the first layer

A uniform thickness of the first layer all over the testing surface:
a) facilitates the calibration procedure of the thermal products and the first layer thickness, as it is performed only for one gauge and applies to all the gauges during the test;
b) and better controls the final dimension of the testing surface.
Thus, the gluing procedure of the first layer onto the model-second layer is performed by a skilled technicial and the uniformity of the first layer thickness is also experimentally controlled through the calibration of two or more gauges.

3.8 Determination of the thermal product by Joule effect (electrical discharge method)

The calibration method using the Joule effect is based on an abrupt submission of the sensor on a high current intensity (step in wall heat flux) for a very short time (less than *10ms*). The test is performed once under air, which is an excellent insulator and for the short experimental times all the heat flux can be considered that goes into the substrate of the gauge (Eq. (22)), and once in a liquid of known thermal product $\sqrt{(\rho ck)}_L$ (Eq. (23)), where part of the heat flux enters the substrate ($Q_{W,L}$) and part of it is diffused in the liquid ($Q_{CONDUCTION\ in\ L}$) (Schultz and Jones, 1973). According to Eq. (9), the total heat flux for each case is given:

$$Q_{joule,AIR} = Q_{W,AIR} = \sqrt{\rho ck} \cdot f_{AIR}\left[T_W(t)\right], \tag{22}$$

$$Q_{joule,L} = Q_{W,L} + Q_{CONDUCTION\ in\ L} = \sqrt{\rho ck} \cdot f_L\left[T_W(t)\right] + \sqrt{(\rho ck)}_L \cdot f_L\left[T_W(t)\right], \tag{23}$$

where, $f_{AIR}\left[T_W(t)\right]$, $f_L\left[T_W(t)\right]$ are functions of wall temperature history. Provided that the one dimensionality and the semi-infinite hypotheses are satisfied, these functions are proportional to square root of time (Eq. (24)):

$$f_M\left[T_W(t)\right] = \frac{\sqrt{\pi}}{2}\frac{\Delta T_{W(M)}(t)}{\Delta\sqrt{t}} = \frac{\sqrt{\pi}}{2}\alpha_{T(M)}, \quad M = AIR \text{ or } L, \tag{24}$$

where $\alpha_{T(M)}$ is the slope of the wall temperature change over the square root of time for the test performed in the air or in the liquid. The magnitude of the heat fluxes generated by Joule effect $Q_{joule,M}$ is given in Eq. (25):

$$Q_{joule,M} = \frac{I_M{}^2 R_M \zeta}{A}, \quad M = AIR \text{ or } L. \tag{25}$$

In case that the current intensity is the same for both tests ($I_{AIR} = I_L$) and the initial temperature level is identical for both experiments ($R_{AIR} = R_L$), the magnitude of the heat fluxes from Joule effect is equal ($Q_{joule,AIR} = Q_{joule,L}$). Note that the area of the gauge A, and the correction factor ζ for non-uniform heating are characteristics of the same sensor.

Both parameters (A, ζ) can not be accurately quantified and they can be disregarded from the calculations by applying the high current intensity twice, once under air and once under a

known liquid. So, according to the above analysis, combining Eq. (22) and Eq. (23), the thermal product of the substrate $\sqrt{\rho ck}$ is given by Eq. (26):

$$\sqrt{\rho ck} = \frac{\sqrt{(\rho ck)_L}}{\frac{\alpha_{T(AIR)}}{\alpha_{T(L)}} - 1} \quad . \tag{26}$$

Maulard (1969) and Schultz and Jones (1973) demonstrated that the optimum ratio of the slopes to give the least error in thermal product $\sqrt{\rho ck}$ determination is $(1+\sqrt{2})$ and thus the liquid should in principle have thermal properties such that:

$$\sqrt{(\rho ck)_L} = \sqrt{2}\sqrt{\rho ck} \quad . \tag{27}$$

Tests were successfully performed by using a Macor substrate of a single-layer gauge in air, and in a liquid such as glycerin or water, whose thermal products are well defined equal to *925* and *1625 J/(m^{2}Ks$^{0.5}$)* respectively. The data reduction time was studied by Denos (1996): a time duration below *2.5ms* for the application of the above one dimensional theory was proposed. During this time, the lateral conduction seems to be very much limited. In addition, for current intensities from *30* to *70mA*, the heat flux from Joule effect could be considered almost constant, as the gauge resistance *R* (whose value is usually between *50-80Ω*) does not increase more than *1Ω*. The sampling frequency was *20kHz* (high enough as the data reduction time is very short). The determination of the zero time t_0 was quite obvious for this case, because of the abrupt increase of the wall temperature once the current is applied on the sensor.

Eventually, the same technique could be used for the calibration of the thermal product of the first layer $\sqrt{(\rho ck)_1}$ in a two-layer gauge, as far as the first layer stays semi-infinite during the data reduction time. For example, according to Eq. (21), when the first layer is Kapton (α = *0.0775x10^{-6}m^2/s*) and the data reduction time is equal to *0.0025s* or *0.002s*, the thickness required to satisfy the semi-infinite condition is *50.8μm* and *45.4μm* respectively. Doorly and Oldfield (1986) calibrated the thermal product of the vitreous enamel coating (first layer) on a mild steel (second layer) equal to *1468J/(m^2 K s$^{0.5}$)*. (The first layer thickness was *200μm.*)

At VKI, tests on two-layer gauges of Kapton (first layer) glued on a metallic substrate overestimated the value of the thermal product of Kapton (whose theoretical value is *431J/(m^2 K s$^{0.5}$)*) The reason can be found in Eq. (27): the theoretical thermal product ratios of glycerin over Kapton and water over Kapton are *2.15* and *3.78*, values far from $\sqrt{2}$ (= *1.414*). On the other hand, glycerin and water are widely used for the determination of the Macor thermal product, with the corresponding ratios over Macor *0.45* and *0.78* (Denos, 1996). Maulard (1969) also recommended glycerine for the quartz thermal product, with the ratio only *0.6*.

The method was not investigated further for the $\sqrt{(\rho ck)_1}$ calibration of the first layer of the two-layer gauge, mainly because even if an accurate determination of $\sqrt{(\rho ck)_1}$ could be possible, still more experiments should be performed for the determination of the thickness of the first layer and the thermal properties $\sqrt{(\rho ck)_2}$ of the second. Hence, a more general experiment is produced for the calibration of all the three parameters at once by using a uniform air jet as a heat flux source. However, the knowledge of $\sqrt{(\rho ck)_1}$ could eventually simplify the calibration with the uniform jet described in the next paragraphs and this is the reason that a chance was given to the electrical discharge method for the $\sqrt{(\rho ck)_1}$ determination.

3.9 Determination of the thermal products and the first layer thickness

3.9.1 Uniform air jet as a heat source

A jet of hot air as a heat source is used for the determination of the two thermal products and the thickness of the first layer similarly to Piccini et al. (2000). The flow is heated at *340K* and exits through a *15mm* diameter nozzle preceded by a settling chamber. In order to control the test conditions, the total pressure and temperature are measured inside the settling chamber of the nozzle. The step function applied to the gauge is obtained with a fast opening shutter placed between the gauge and the nozzle exit. Preliminary measurements of temperature, velocity and turbulence intensity for several distances from the end of the nozzle are performed (Ferrara, 2002). At an axial distance of a nozzle diameter (*15mm*) downstream of the nozzle, the aero–thermal conditions are reasonably constant over 80% of the diameter (potential core). This ensures the one dimensional hypothesis over the test duration.

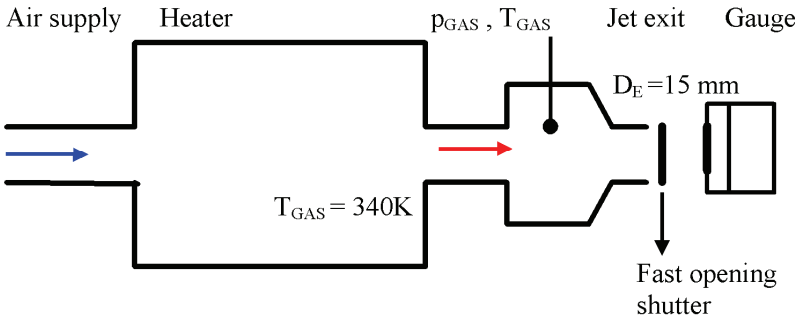

Figure 3-5: Calibration set-up

A number of gas temperature steps are applied to the gauge for various jet velocities. The heat transfer coefficient is determined using a reference Macor gauge for which the thermal product was already calibrated by Joule effect (paragraph 3.8), (*2073 J/(m^{2}Ks$^{0.5}$)* - Denos, 1996). First, the wall heat flux evolution is determined using the numerical solution based on the Crank-Nicholson scheme. Then, the heat transfer coefficient history, *h(t)*, during the experiment is calculated from its definition (Eq. (28)). The constant pressure and temperature of the jet flow result in a constant heat transfer coefficient, *h*:

$$h(t) = \frac{Q_W(t)}{T_{GAS} - T_W(t)}\ , \tag{28}$$

$$Nu = \frac{hD_E}{k_{GAS}} = \frac{Q_W(t)D_E}{k_{GAS}\left(T_{GAS} - T_W(t)\right)}\ . \tag{29}$$

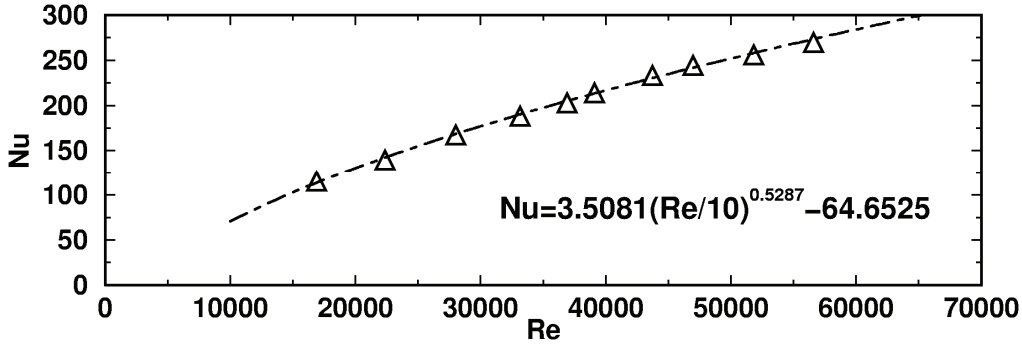

Figure 3-6: Nusselt-Reynolds number correlation obtained with single-layer thin-film gauge (Iliopoulou et al., 2004)

A correlation of Nusselt number (Eq. (29)) as a function of Reynolds number (based on the nozzle diameter) is then produced and showed in Figure 3-6. Note the test-to-test repeatability is better than *1%* (Billiard et al., 2002).

3.9.2 Calibration algorithm

Once the air jet is well defined, the two-layer gauge is introduced to this known heat source, $Q_W(t)$, and the sensor's response from the new test is monitored, $T_W^T(t)$. This new test is graphically represented in Figure 3-7, as the 'Real System'. A minimization routine based on a quasi-Newton algorithm, available from a mathematical library Nag, which is indicated as the 'Model Fitting' in Figure 3-7, modifies the two thermal products and the thermal thickness of the first layer (that are the three guessed parameters) at every iteration and compares the analytical solution (Eq. (11)) (or the numerical one that is described in paragraph 3.6 depending on the choice of the mathematical model, see Figure 3-7), with the experimental data until a good fit is obtained (Billiard et al., 2002). In case that the analytical solution from Eq. (11) is used as mathematical model, the monitored response of the gauge in the air jet, $T_W^T(t)$, is firstly modified from a step in fluid temperature to a step in wall heat flux (paragraph 3.5); the input heat source corresponds to a constant wall heat flux with initial heat transfer coefficient *h* (for zero time) equal to the value of the air jet experiment and the monitored wall temperature is transformed to the superimposed wall temperature that corresponds to the constant wall heat flux.

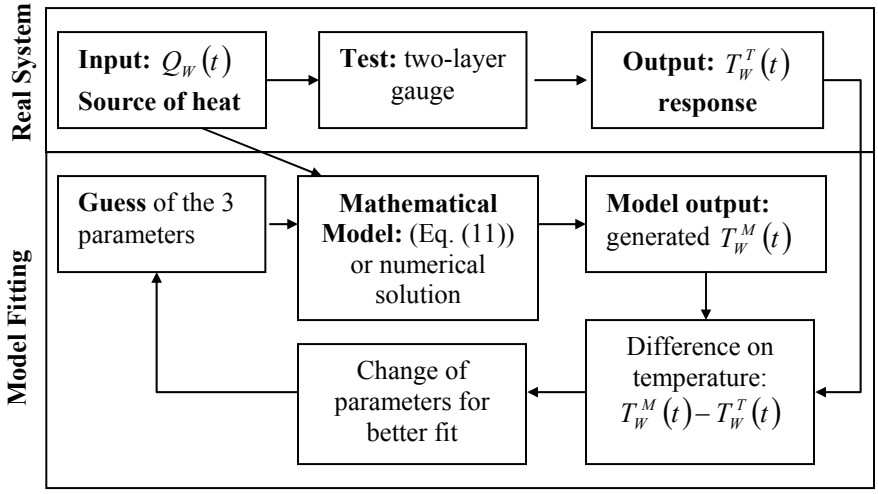

Figure 3-7: Optimization algorithm principle (Billiard et al., 2002)

In order to test the calibration algorithm, a wall temperature signal is generated from Eq. (11), which corresponds to the test case of the real system. The values of the thermal products, the thickness and the wall heat flux are selected identical to that of Figure 3-2. Pretending that the three above parameters were unknown, the calibration algorithm is applied on the generated wall temperature signal, by using as a mathematical model the numerical solution. The model fitting is able to find the three parameters with a fitting capacity of *0.05%*. The above procedure is demonstrated at the left side of Figure 3-8. The top graph illustrates the numerically generated wall temperature signal and the best fit calculated by the calibration algorithm. The bottom graph shows the difference between the two above temperature signals.

After the calibration algorithm is validated, it is used for the calibration of several configurations of gauges. In Figure 3-8, one example is demonstrated graphically (Ferrara, 2002):

the wall temperature is measured by a two-layer thin-film gauge and it is corrected with the superposition technique, for constant wall heat flux (dashed red line on the top-right graph). Then it is fitted with the analytical solution using the iterative optimization routine. The calibration results provide *747* and *2146 J/(m²Ks^0.5)* for the first layer Upilex-S and the second layer Macor thermal product and *303μm* for the thickness of the first layer. (Theoretical values: $\sqrt{(\rho ck)_{1,2}}$ = *692, 1780 J/(m²Ks^0.5)*. Manufacturer value: *250μm*) Note that *2sec* of experimental time is found to be close to the upper limit, where the heat conduction inside the gauge can still be considered as one dimensional.

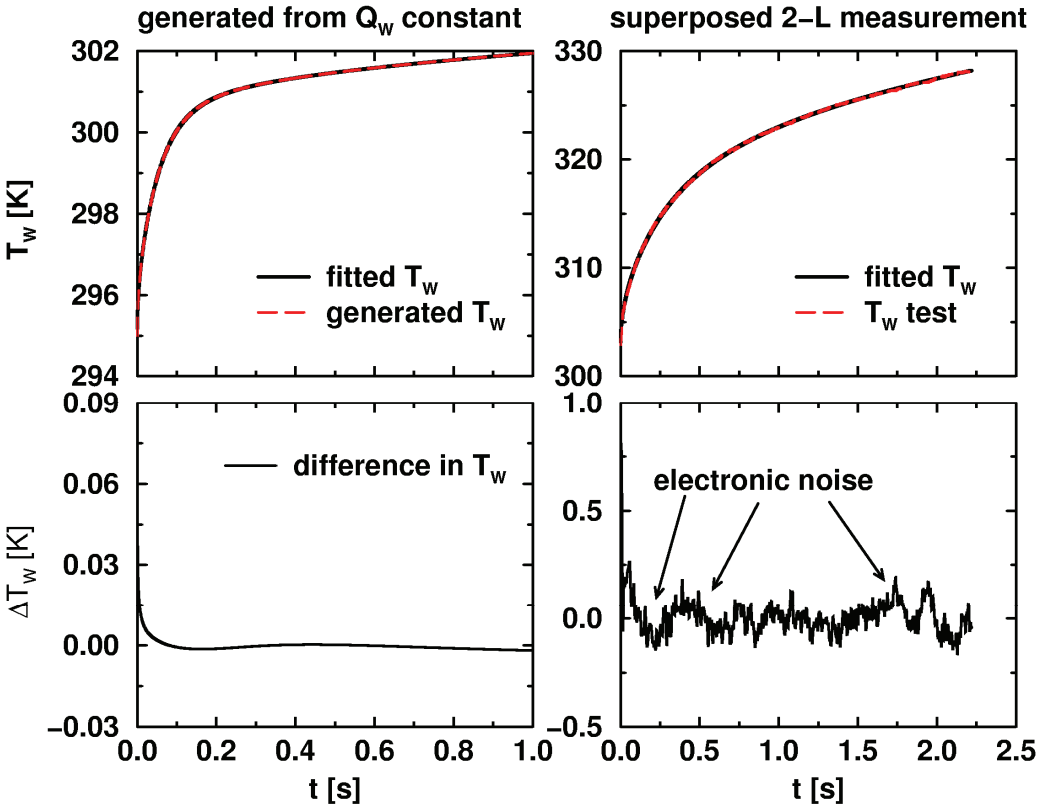

Figure 3-8: Validation of the calibration algorithm (left) and an example of calibration (right)

As shown in Figure 3-7, the wall heat flux source should be well defined, because it is the input to the mathematical model; then the model output $T_W^M(t)$ is influenced only by the three parameters. In general, the wall temperature history is a function of these three parameters and the wall heat flux (e.g. Eq. (11)). An imprecise wall heat flux forces the optimization algorithm to produce imprecise values for the three parameters. Thus, it is necessary that the wall heat flux history can be accurately characterized. At VKI, it is characterized through the heat transfer coefficient *h* (Eq. (28), which results from the correlation determined previously by the single-layer gauge (see Figure 3-6).

The determination of the applied wall heat flux by Joule effect for the thermal product calibration of the single-layer gauge is avoided by employing a liquid of known thermal properties (paragraph 3.8). The equivalence between the two calibration techniques is obvious: the calibrated parameters of the two-layer gauge are based on the single-layer thermal product, which is furthermore based on the known thermal properties of a liquid.

Except from electrical (paragraph 3.8) and convective (paragraph 3.9.1) heating, the wall heat flux source for the thermal product calibration of the gauge can also be radiative. This technique consists of a LASER as the heat source, as done by Lyons and Gai (1988) for single-

layer gauges and Thorpe et al. (2000) for two-layer gauges. The first advantage is that the beam covers a large area around the gauge, so that the one dimensional conduction assumption remains valid for longer durations. The second advantage is the abrupt generation of a step in the wall heat flux (approximately in *1ms*) that facilitates the determination of time t_0 (thus the analytical solutions of the paragraphs 3.3.2 and 3.4 can easily be employed). This method was also evaluated at VKI (Galvan, 2001) but even if the power emitted by the LASER is well known, it differs from the one received by the gauge because of reflection. Additionally, the reflection is different on the gauge and on the substrate.

3.9.3 Calibration results

Three types of two-layer thin film gauges are made according to the material of their second layer: Macor, quartz and steel. The first layer for all the three gauges is Upilex-S (a polyimide sheet that can easily be glued on the above second layers). Concerning the Macor test piece, two layers of glue and Upilex are used. The purpose is to check if the glue layer can be distinguished from the Upilex and to enlarge the portion of the time history where only the influence of the Upilex/glue assembly is tested. The mathematical model of the calibration algorithm (Figure 3-7) is based on the numerical solution (paragraph 3.6). The results are presented in Table 3-1 together with the manufacturer and the test-to-test repeatability (Billiard et al., 2002).

The tests with two successive layers of glue and polyamide did not reveal any inflexion point in the wall temperature history confirming thus that the thermal properties of the glue and the polyamide are very similar.

	$\sqrt{(\rho ck)_1}$ Upilex [J/m^{2}Ks$^{0.5}$]	Upilex Thickness [µm]	$\sqrt{(\rho ck)_2}$ second layer [J/m^{2}Ks$^{0.5}$]
on *Macor* (8 tests)	731	305	2117
Manufacturer value	692	250	1780
on *quartz* (9 tests)	752	167	1726
Manufacturer value	692	125	1521
on *steel* (5 tests)	699	175	8147
Manufacturer value	692	125	8088
	Difference between calibration results and manufacturer value in percentage [%]		
on *Macor* (8 tests)	5.6	22	19
on *quartz* (9 tests)	8.6	34	13
on *steel* (5 tests)	1.0	40	0.7
	Dispersion of the calibration results (20:1) [+/-%]		
on *Macor* (8 tests)	2.3	3.9	5.9
on *quartz* (9 tests)	3.9	3.9	4.9
on *steel* (5 tests)	8.8	8.7	9.0

Table 3-1: Calibration results compared to the manufacturer values

Regarding the average calibrated values of the thermal product of Upilex, the differences with respect to the manufacturer values are *+5.6%*, *+8.7%* and *+1%* for the samples glued on Macor, quartz and steel respectively. The value obtained for Macor (*2117 J/(m^{2}Ks$^{0.5}$)*) is naturally close to the one determined by electrical heating (*2073 J/(m^{2}Ks$^{0.5}$)*), which is the value used for the thermal product of the reference gauge that provides the Nusselt-Reynolds number correlation

(Figure 3-6). The large overestimation with respect to the manufacturer data (*+19%*) was also observed by Miller (1981) with the electrical heating technique. The thermal product of quartz differs by *+13%* from the manufacturer data. For steel, a good agreement is obtained (less than *1%* difference). As far as the Upilex thickness is concerned, its calibrated values are far from the actual values of the Upilex sheet before being glued on the second substrate. Note that during the gluing procedure, pressure is applied everywhere on the Upilex top surface, except of the close region of the gauge, possibly implying that few sporadic air bubbles are accumulated between the first and the second layer in the gauge region. The high difference between the calibrating results and the manufacturer values shows the importance of the thermal product calibrations of the gauge substrates, because only accurate values lead to accurate wall heat flux calculations during a measurement (paragraphs 3.3 and 3.4).

The repeatability obtained on the thermal product of Upilex is satisfactory on Macor (± *2.3 %*) and on quartz (± *3.9 %*). The repeatability obtained for the thermal products of Macor and of quartz *(*± *5.9%* and ± *4.9%*) is reasonable. For the tests on steel, the repeatability is not as good as for the rest of the cases. The low number of tests includes calls for a new calibration with more tests, which is commented in the next paragraphs. In general, the repeatability on the tests is much better than the uncertainty on the mean value of the thermal product. Another interesting point for performing a number of tests is to increase the confidence on the calculated mean values. If σ is the confidence on a single test, the confidence on the mean is $\sigma/\sqrt{n}$, where *n* is the number of the tests (Wonnacott and Wonnacott, 1985).

The repeatability on the results obtained by this technique is much better than that obtained by the analytical solution for constant heat flux (Eq. (11)). Firstly, in the latter case, the time t_0 at which the step starts (see 3.7.4) must be defined with accuracy. This is not obvious since the experiment is never a perfect step. Moreover, the higher accuracy of the numerical model is probably due to the fact that there is no need to compensate the temperature signal to a pseudo constant heat flux. The gas temperature could even vary. Examples where the heat transfer coefficient is not constant during the calibration tests are demonstrated in the next paragraphs.

3.9.4 More details about the calibration procedure – Calibration of the stagnation gauge

The two-layer substrate thin film gauges are implemented on a blade of the second stator in the one and a half stage turbine of the VKI I.L.P. facility, CT3. The commercial gauge used in this work is bought from Tao Systems, where it is called as Senflex Multi-element Surface Hot-film Sensor. However, at VKI, it is used as thin film gauge that operates in constant current mode (paragraph 2.2.1) for heat transfer measurements. Note that at VKI, the first use of the Senflex gauge was carried out by Iliopoulou (2000); previous research on two-layer gauges was performed by Pelle and Arts (1997) on gauges manufactured at the University of Louvain (UCL). The Senflex gauge consists of a *2.5mm* serpentine nickel thin-film, with a resistance of *60Ω*, painted on a *50μm* thick Upilex-S sheet that can be glued on the blade surface with a *75μm* thick double-sided adhesive sheet. A schematic representation of the gauges together with the blade is shown in Figure 3-9.

The calibration results of Upilex glued on steel in Table 3-1 (third case) are used for the wall heat flux calculations of the measurements in the CT3 facility with the instrumented stator blade of Figure 3-9 (see chapter 5). The calibration of Table 3-1 is performed on one of the gauges at the suction side of the blade, where the curvature effects are negligible. However, the gauge situated in the stagnation region of the blade is in the most highly curved region. Thus, in order to ensure that the values of all the three parameters (the two thermal products and the thickness of Upilex-S) are also valid for the stagnation region of the blade, the calibration is repeated for the stagnation gauge. A new second heat flux source is used and is characterized by

another single-layer gauge fired onto a ceramic insert substrate (Macor) deposited at the stagnation region of a similar airfoil.

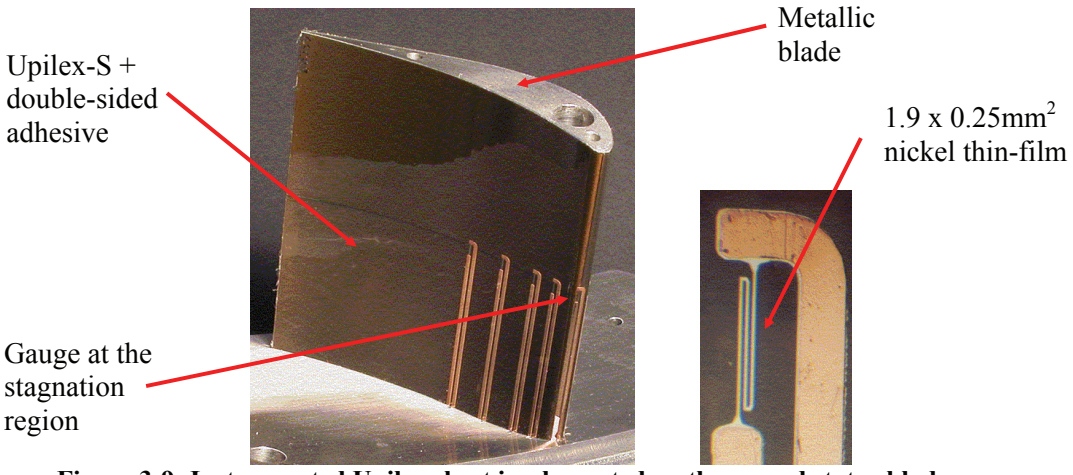

Figure 3-9: Instrumented Upilex sheet implemented on the second stator blade

For the stagnation gauge calibration, contrary to the calibration of the gauge at the suction side of the blade (paragraph 3.9.3), the iterations of the calibrated parameters are based on the wall heat fluxes comparison (from the single-layer gauge experiment – characterization of the jet – and from the two-layer gauge experiment together with the three guessed parameters, see Figure 3-7). The numerical solution based on the Crank-Nicholson scheme is used as the mathematical model for the stagnation gauge calibration. Two of the calibration tests are shown in Figure 3-10. The top graphs illustrate the well known wall heat flux (black line) and the best fit that the calibration algorithm calculates (red line), for two different test cases (left and right graph). The bottom graphs show the difference of the two above heat flux signals for each test case. The new calibration results are shown in Table 3-2. The calibration is repeated several times and the calibration results are within the dispersion of Table 3-1. Note, that the higher noise, which is observed for the well known heat flux, is due to the higher noise on the wall temperature history measured by the single-layer gauge.

The main conclusion is that the calibration can be applied to only one of the gauges of the blade and the values of the three parameters are valid for any other gauge, as far as all gauges come from the same manufacturing procedure at the same time.

	$\sqrt{(\rho ck)_1}$ Upilex [J/m²Ks$^{0.5}$]	Upilex Thickness [μm]	$\sqrt{(\rho ck)_2}$ second layer [J/m²Ks$^{0.5}$]
First test (left of Figure 3-10)	692	173	7763
Second test (right of Figure 3-10)	713	162	8888
Manufacturer value	692	125	1780

Table 3-2: Calibration results at the stagnation gauge

The main advantage of the use of the numerical solution for the calibration algorithm is that no constrains on the wall heat flux or on the heat transfer coefficient, *h*, are needed. *"h"* can follow any kind of history, as far as this history can be reconstructed twice, once measured with a test by using a single-layer gauge and once applied as boundary condition to the calibration test of the two-layer gauge.

For the stagnation gauge calibration, a second nozzle of *20mm* diameter is employed. The exit of this nozzle is followed by a shutter placed only few millimeters further. (Behind the shutter, the blade with the stagnation gauge is put). The other side of the nozzle is connected to a big rest chamber; the latter is filled with the constant pressure line of 7 bars. The set up is similar with that of Figure 3-5, the only difference is the added big rest chamber. When the shutter is closed, the chamber gets pressurized, due to the small exit area of the flow that passes between the nozzle exit and the shutter compared to the 7 bars line diameter. However, when the shutter opens, the pressurized air suddenly discharges, because the exit nozzle diameter is bigger than the one of the 7 bars line (top left graph of Figure 3-11). As a result, there is a higher Nusselt number exactly after the opening of the shutter, which becomes constant in less than half a second. Then a new equilibrium between the flow that enters the chamber from the 7 bars line and the flow at the exit of the nozzle takes place. Please, notice that once the flow is established, the Nusselt number can be considered constant for the next second.

In case that the experiment is performed for longer time, the Nusselt number history will start rise, not because the flow conditions are not uniform, but mainly due to lateral conduction effects in the gauges substrates. The numerical solution is not able to take into account these lateral effects, as it is the solution of the one dimensional conduction equation (Eq. (3)).

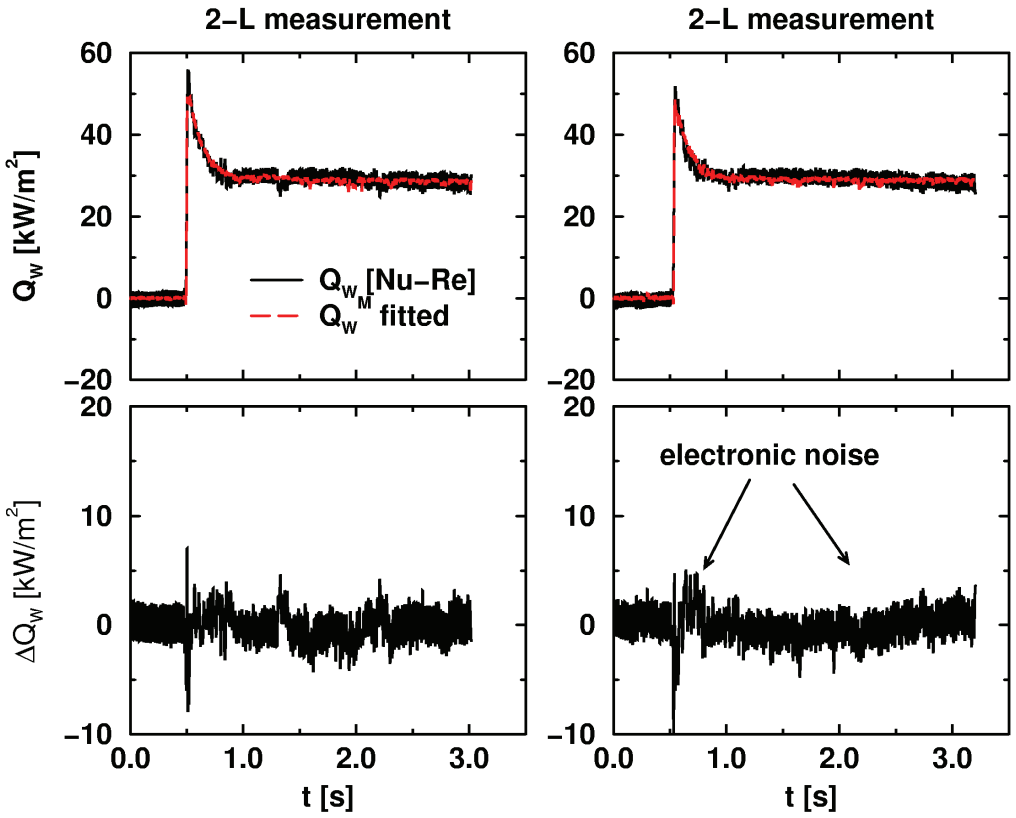

Figure 3-10: Two examples of calibration tests for non-constant wall heat flux

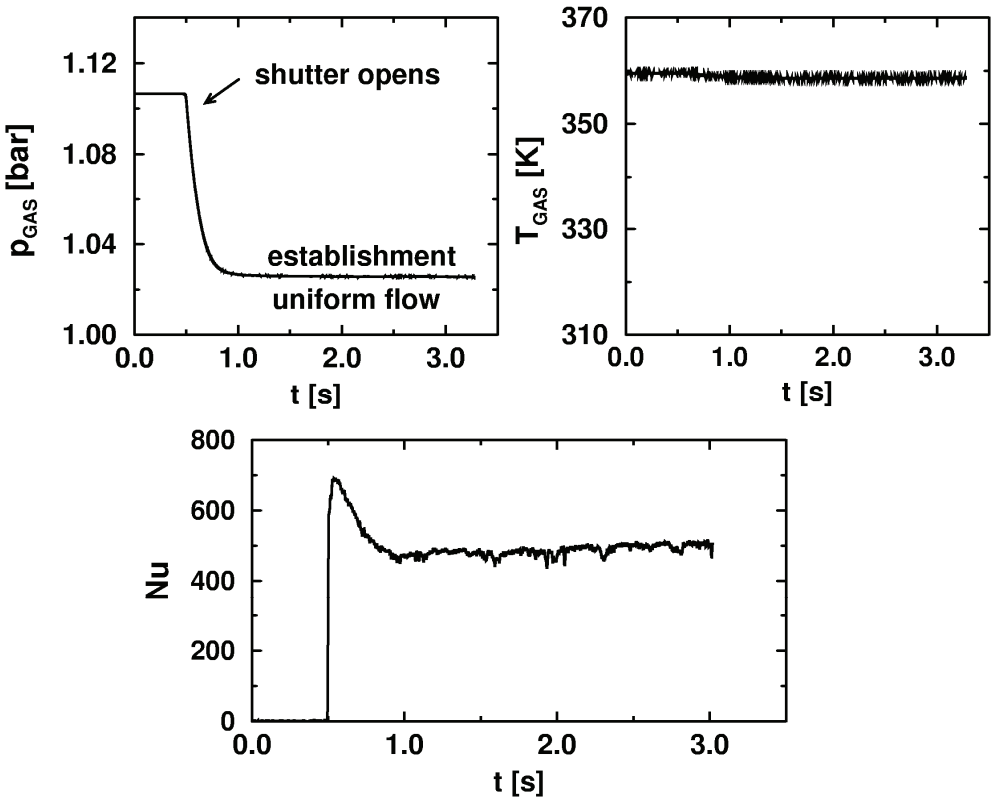

Figure 3-11: Flow conditions and Nusselt number history for some of the calibration tests

3.10 References

Ainsworth R.W., Allen J.L., Davies M.R.D., Doorly J.E., Forth C.J.P, Hilditch M.A., Oldfield M.L.G., Sheard A.G., 1989, *'Developments in Instrumentation and Processing for Transient Heat Transfer Measurement in a full-Stage Model Turbine'*, J. of Turbomachinery, vol. 111, pp 20-27

Billiard N., Iliopoulou V., Ferrara F., Denos R., 2002, *'Data reduction and thermal product determination for single and multi-layered substrates thin-film gauges'* Proceeding of the 16th Symposium on Measuring Techniques for Transonic and Supersonic Flows in Cascades and Turbomachines, Cambridge, Great Britain

Denos R., 1996, *'Aerothermal investigation of the unsteady flow in the rotor of a transonic turbine stage'*, Ph.D. thesis, University of Poitiers, France

Doorly J.E., Oldfield M.L.G., 1986, '*New heat transfer gages for use on multilayered substrates.',* J. of Turbomachinery, Vol.108, pp 153-160

Ferrara F., 2002, *'Assessment of a heat flux source for the determination of thin film gauge substrate thermal product'*, VKI SR 2002-15

Galvan I., 2001, *'Assessment on the use of a LASER to determine the thermal product of thin-film gauge substrates'*, VKI PR 2001-11

Iliopoulou V., 2000, *'Optimization of double-layer thin film gauges for heat transfer measurements'*, VKI PR 2000-27

Iliopoulou V., Denos R., Billiard N., Arts T., 2004, *'Time averaged and time-resolved heat flux measurements on a turbine stator blade using two-layered thin-film gauges'*, ASME 2004-GT-53437, Vienna, Austria – J. of Turbomachinery, vol. 126, pp 570-577

Lyons P.R.A., Gai S.L., 1988, *'A method for the accurate determination of the thermal product $(\rho ck)^{1/2}$ for thin film heat transfer or surface thermocouple gauges'*, J. of Phys. E: Sci. Instrum., vol. 21, pp 445-448

Maulard J., 1969, *'Etude du fluxmètre à température superficielle pour mesures dans les tubes à choc'*, ONERA NT 139, 1969

Miller C.G., 1981,, *'Comparison of Thin-Film Resistance Heat-Transfer Gages With Thin-Skin Transient Calorimeter Gages in Conventional Hypersonic Wind Tunnels'*, NASA Technical Memorandum 83197, December 1981

Pelle O., Arts T., 1997, *'Development of a double-layer thin film gauge for surface heat transfer measurements'*, Proc. of Eurotherm Seminar 55, Heat transfer in single phase flows 5, Santorini, Greece

Piccini E., Guo S.M., Jones T.V., 2000, '*The development of a new direct-heat-flux gauge for heat-transfer facilities'*, J. of Measurement Science and Technology, vol. 11, pp 342-349

Schultz D.L., Jones T.V., 1973, '*Heat transfer measurements in short duration hypersonic facilities'*, AGARDograph Report 165

Thorpe S.J., Yoshino S., Ainsworth R.W., 2000, *'Fabrication and calibration techniques for turbine rotor tip heat transfer gauges'*, Proceedings of the XV Symposium on Measuring Techniques for Transonic and Supersonic Flows in Cascades and Turbomachines, Florence, Italy

Wonnacott R.J., Wonnacott T.H., 1985, *'Introductory statistics'*, John Wiley & Sons, Inc, Fourth edition, ISBN 0-471-86899-X